Partial Discharge Behavior of High Frequency Transformer Insulation under High Voltage PWM Stress

Wang, Zhaoxin; Wei, Xing; Bak, Claus Leth; da Silva, Filipe Faria; Luo, Tianming; Zhao, Weichuan; Vaessen, Peter; Sorensen, Henrik; Niasar, Mohamad Ghaffarian

DOI
10.1109/TPEL.2025.3566999

Publication date
2025

Document Version
Final published version

Published in
IEEE Transactions on Power Electronics

Citation (APA)
Wang, Z., Wei, X., Bak, C. L., da Silva, F. F., Luo, T., Zhao, W., Vaessen, P., Sorensen, H., & Niasar, M. G. (2025). Partial Discharge Behavior of High Frequency Transformer Insulation under High Voltage PWM Stress. *IEEE Transactions on Power Electronics*, *40*(9), 13142-13156. https://doi.org/10.1109/TPEL.2025.3566999

Partial Discharge Behavior of High-Frequency Transformer Insulation Under High-Voltage PWM Stress

Zhaoxin Wang, *Member, IEEE*, Xing Wei, *Member, IEEE*, Claus Leth Bak, *Senior Member, IEEE*, Filipe Faria da Silva, *Senior Member, IEEE*, Tianming Luo, *Member, IEEE*, Weichuan Zhao, Peter Vaessen, *Member, IEEE*, Henrik Sørensen, and Mohamad Ghaffarian Niasar, *Member, IEEE*

***Abstract*—As the voltage levels of solid-state transformers (SSTs) increase using medium-voltage switches, high-frequency transformers (HFTs) used inside SSTs are subjected to increased electrical stress. This stress, characterized by high voltage, high-frequency pulsewidth modulation (PWM) voltage, can cause insulation partial discharge (PD) and potentially lead to failure of the HFT insulation system. While PD behavior under power-frequency sinusoidal voltage has been extensively studied, the behavior of HFT insulation under PWM square pulse conditions is less well understood. To address this gap, a high voltage high-frequency PWM voltage PD test platform is developed and high-frequency current transformer (HFCT) and ultra-high-frequency (UHF) antenna are used for PD signal detection. PD tests are performed under a variety of PWM conditions including PWM frequency, rise time, voltage amplitude, and different insulation layers to thoroughly investigate the HFT insulation behavior. The PD characteristics of repetitive PD inception voltage and phase-resolved PD patterns at different PWM conditions are recorded and analyzed under PWM conditions. In addition, this article explores the underlying PD mechanisms of the HFT insulation under high-frequency PWM stress, providing insights to explain the observed test results. The findings from this research provide essential references and lay a solid foundation for future advances in optimal design, health monitoring, reliability analysis, and lifetime prediction for HFTs in power electronics applications.**

***Index Terms*—High-frequency transformer (HFT), insulation, pulsewidth modulation (PWM) stress, partial discharge (PD), triple junction (TJ).**

I. Introduction

THE advance in power electronics technology have led to an increase in the operating voltage levels of power electronic converters [1], [2], [3]. As a key component of the dc–dc converter, the high-frequency transformer (HFT) faces the significant challenge of withstanding high-frequency (HF) and high-voltage pulsewidth modulation (PWM) stress. This PWM stress, characterized by rapid switching and high voltage levels, can potentially contribute to accelerated aging and discharge of the HFT insulation, threatening converter reliability [4], [5], [6].

A critical concern within the HFT is the triple junction (TJ), a junction of insulation, winding, and air [7]. As shown in Fig. 1, the TJ is particularly susceptible to insulation degradation and partial discharge (PD) due to the different electrical properties

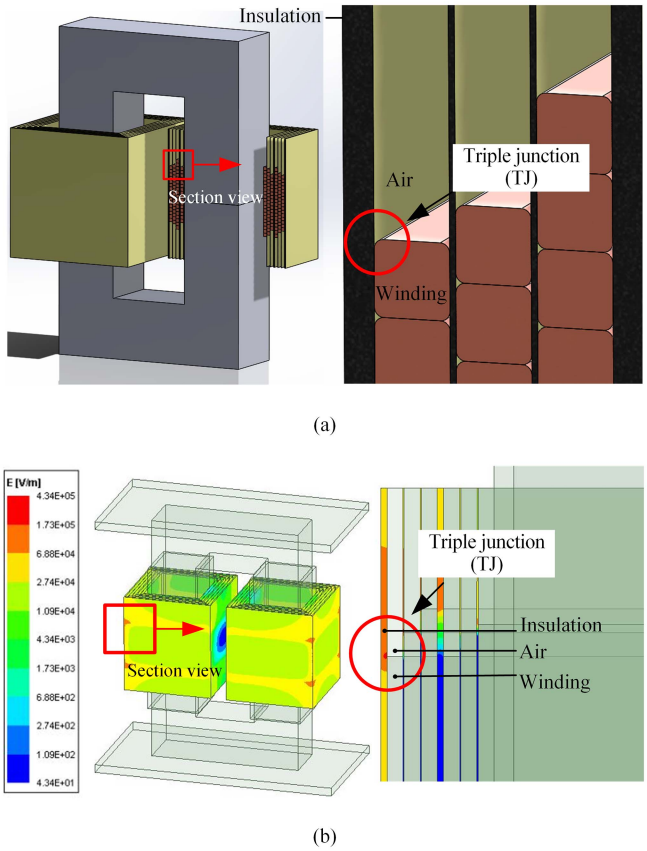

Fig. 1. Diagram of the TJ. (a) TJ of winding, insulation, and air. (b) Electric field distribution of the HFT with TJs [10].

Received 21 January 2025; revised 15 March 2025; accepted 26 April 2025. Date of publication 6 May 2025; date of current version 30 June 2025. Recommended for publication by Associate Editor K. Ngo. *(Corresponding author: Xing Wei.)*

Zhaoxin Wang, Xing Wei, Claus Leth Bak, Filipe Faria da Silva, and Henrik Sørensen are with AAU Energy, Aalborg University, 9220 Aalborg, Denmark (e-mail: zwa@energy.aau.dk; xwe@energy.aau.dk; clb@energy.aau.dk; ffs@energy.aau.dk; hs@energy.aau.dk).

Tianming Luo, Weichuan Zhao, Peter Vaessen, and Mohamad Ghaffarian Niasar are with the Department of Electrical Sustainable Energy, Delft University of Technology, 2628 CD Delft, The Netherlands (e-mail: tialu@dtu.dk; zhaoweichuanxjj@gmail.com; P.T.M.Vaessen@tudelft.nl; M.Ghaffarian Niasar@tudelft.nl).

Color versions of one or more figures in this article are available at https://doi.org/10.1109/TPEL.2025.3566999.

Digital Object Identifier 10.1109/TPEL.2025.3566999

TABLE I
OVERVIEW OF PD DETECTION METHODS

PD detection methods	Methods	Reference	Principle	Advantages	Limitation for PWM PD measurement
Electrical methods	Coupling Capacitor	[18]	Measures the PD displacement current through a coupled capacitor.	High sensitivity, and fast detection speed.	Affected by electromagnetic interference, and susceptible to noise.
	HFCT	[20], [21], [22], [23]	Detects high-frequency currents induced by PD events.		
Electromagnetic detection method	UHF Antenna	[25], [26], [27], [28], [29], [30]	Capture electromagnetic waves emitted by PD in the UHF range.	High sensitivity, fast detection speed, improved immunity against interference, and non-destructive and non-intrusive.	Requiring postprocessing.
Optical detection methods	Optical Detection (Using PMT or fluorescent fibers)	[32], [33], [34]	Detects PD through the observation of radiation photons emitted during discharge.	High sensitivity, fast detection speed, fully isolated from electrical disturbances, immunity to electromagnetic interference, and non-destructive and non-intrusive.	Requires direct line of sight to the PD source, and relatively expensive and complex setup.
Other methods	Acoustic Detection	[35]	Uses acoustic emissions generated by PD.	High sensitivity, immunity to electromagnetic interference, and non-destructive and non-intrusive.	Low detection speed, complex calibration, and susceptible to environmental noise.
	Ultrasound and Ozone Sensors	[36]	Detects chemical by-products of PD through ultrasound and ozone sensors.	Can identify specific by-products of insulation degradation.	Secondary-response detection results in low detection speed, and complex calibration.

of the materials that converge at the junction [8], [9]. These differences result in nonuniform electric fields and stress concentrations that increase the risk of PDs occurring [10]. Once PD initiates, the insulation material at the TJ begins to degrade as a result of repeated PD events. Each PD event causes localized damage due to the energy impact of high-energy electrons or accelerated ions, leading to chemical transformations in the insulating material [8]. This degradation can accelerate insulation breakdown, reducing the overall life of the insulation system.

Encapsulating windings in dielectric materials such as epoxy resin or oil is a common approach to prevent PD. However, the optimized design of HFTs requires careful consideration and tradeoffs between multiple factors, including heat dissipation, maintenance, system integration, power density, and insulation coordination [11], [12]. HFTs with insulation and windings exposed to air are potential designs to consider. Several optimized design solutions have been proposed for medium to HFTs, utilizing solid dielectrics between winding layers, with air as the surrounding medium [13], [14], [15].

To address this critical issue, this study focuses on investigating the PD characteristics at the TJ of the HFT under the condition of HF and high-voltage PWM stress.

While broad knowledge of PD has been achieved under power frequency sinusoidal voltage, investigations into PD behavior under increasingly HF PWM conditions have been less comprehensive. Compared to traditional PD detection at power frequencies, PWM voltage presents new challenges. The HF and fast rise and fall rates of PWM signals generate pronounced electromagnetic interference (EMI), making PD detection difficult [16]. In addition, in order to study this phenomenon, a high-voltage PWM generator with adjustable voltage, frequency, and rise time is also required.

In order to effectively and accurately detect PD signals under PWM voltage, PD detection methods are reviewed and summarized in Table I, including their principles, advantages, and limitations for PWM PD detection. PD detections and measurements are feasible due to the distinguished physical phenomena, which can be categorized including electrical, ultra-high-frequency (UHF) techniques, optical methods, and other methods [17].

A. *Electrical Detection Methods*

Electrical detection, which includes coupling capacitor techniques and high-frequency current transformer (HFCT), provides standardized approaches to PD measurement under AC conditions [18]. HFCT is sensitive to the HF current impulses generated by PD, but it suffers from severe EMI due to switching inrush currents, which means an additional process is needed for the differentiation of PD signals from noise [19].

Research efforts are increasingly directed toward understanding PD characteristics under PWM stress using various electrical detection methods. Zang et al. employed HFCT to perform PD tests of typical defects in power equipment under the staircase waveform. The phase-resolved PD (PRPD) patterns and the pulse repetition rate across various voltage conditions are studied. The results demonstrate different sensitivities of different defects to the staircase voltage, offering invaluable insights for the diagnosis of PD under novel electrical stress scenarios anticipated in future flexible electric grids [20].

Self verified a model for predicting the PDIV of twisted-pair magnet wires (TPMWs), using an HFCT and a C-series sensor to detect PD signals. This research focuses on extensive PDIV measurements of TPMWs coated with various dielectric materials. The study confirms that PDIV can be accurately predicted using the relative permittivity and thickness of the coatings, with frequency effects solely due to permittivity changes with frequency [21].

Liu investigated the PD characteristics of oil–paper insulation subjected to HF electrical stress. To detect PD signals, the techniques of pulse current measurement and HFCT were employed. The experimental findings revealed the presence of

a frequency-induced inflection point around 10 kHz, where PD parameters under HF voltages were significantly higher compared to those under ac voltages. Further investigation into the physical mechanism behind this inflection point revealed that frequency variations influence the charge decay time constant and the residual charge on the insulation surface. These changes affect the charge transport mechanism, leading to alterations in the initial electron generation process and carrier mobility [22].

Liu developed an experimental platform for studying PD in a high-voltage insulated-gate bipolar transistor module. PD measurements for three samples were conducted using an HFCT. Based on the current signals obtained, a novel method for extracting PD pulse currents that did not require the use of additional detection tools is proposed. This approach enabled the accurate extraction of PD pulses from the three samples, even in the presence of displacement currents. The distinct PD characteristics observed across the three typical structures facilitated the identification of different discharge types. The discharge mechanism and its associated characteristics within silicone gel are qualitatively elucidated by analyzing the combined influences of applied voltage and space charge, along with the impact of bubble volume changes within the gel [23].

B. Electromagnetic Detection Method

Electromagnetic detection via UHF antennas captures PD-emitted electromagnetic waves within the UHF spectrum [24]. This principle makes this technique particularly beneficial in environments where high-speed switching EMI is present, as PD can extend beyond the GHz range, beyond the prevailing interference, which is typically below several hundred MHz [25].

Zheng and Ding utilized UHF antennas for PD detection under PWM conditions, investigating the effects of environmental factors such as pressure and temperature on PD characteristics.

Zheng studied the influence of pressure on the PD behavior of polyimide insulation under PWM voltage. A PD test platform was introduced to facilitate PD tests under repetitive unipolar pulse voltage conditions. The platform uses a half-bridge power electronics module to generate the unipolar voltage waveforms and incorporates a pressure tank to provide a controlled pressure environment during the test. The study investigated PD behavior, including PDIV, PD magnitude, and time lag under different pressures. The results indicate that PD inception voltage (PDIV) decreases as pressure decreases. However, the changes in PD magnitude and time delay do not follow a monotonic pattern [26].

Ding focused on PD in high-voltage packaging insulation under square pulses with a high slew rate. A down-mixing PD detection method was proposed, and the influence of temperature on the PD characteristics of power module packaging insulation was explored. The results show that PDIV decreases with increasing temperature. Notably, the PDIV under square-wave conditions consistently exceeds that observed under ac voltage. In addition, a lower slew rate and longer pulse width of the square pulse correspond to a reduction in PDIV [25].

Benmamas investigated the impact of PWM power supply parameters on the PDIV of a simple twisted pair of enameled wires, utilizing antenna sensors for PD signal detection. The study's results indicate that the PDIV is principally determined by the waveform of the voltage oscillations. Specifically, voltage oscillations at lower frequencies are more likely to induce PD. Furthermore, the shape of the waveform is primarily influenced by the rise time of the voltage and the length of the power cable. Another critical factor affecting PD occurrence is the duty cycle; notably, a low duty cycle in unipolar power settings tends to promote the development of PD [27].

Guo studied the PD characteristics of twisted Litz wire and PCB windings under PWM excitations. A novel $\pm$ 5 kV GaN-based HF PWM power supply was developed to investigate the PD behavior of insulation materials under HF bipolar PWM pulses. Both an HFCT and an antenna were used to detect PD signals. PD tests were conducted under PWM conditions up to 5 kV and 50 kHz. The study studied PD behavior, including PDIV, PD charge, and the number of PD occurrences. The results indicate that, in addition to PWM voltage amplitude, both dv/dt and PWM frequency significantly affect PD phenomena. A faster dv/dt decreases the repetitive partial discharge inception voltage (RPDIV) and results in higher PD charges, while an increase in frequency has the opposite effect [28], [29].

Jarrar studied the PD behavior in a back-to-back turn insulation sample and a single cavity layered insulation. A PD test platform was developed with a high-voltage pulse generator capable of producing unipolar square repetitive impulses up to 4 kV with a switching frequency of up to 4 kHz. The PD signals are captured using an octave horn antenna. The study investigated the effects and interactions of applied voltage, switching frequency, rise time, and overshoot on maximum PD magnitudes and PD occurrence rates over time. The results indicate that within the reported parameter range, switching frequency, and overshoot are the primary factors influencing turn insulation life, while the effect of rise time is minimal [30].

Florkowski investigated the influence of a magnetic field on PD dynamics in electrical insulation under PWM excitation. A test platform was developed for PD measurement under PWM excitation in the presence of a magnetic field, with an antenna used to detect PD signals. The setup employed a high-voltage amplifier controlled by a programmable generator, enabling switching frequencies up to 1 kHz and test voltages up to 1.2 kV. The quantitative effect of the magnetic field was captured through phase-resolved acquisition and visualization on time-sequence intensity diagrams. The results indicate that increasing the PWM carrier frequency enhanced PD intensity, which was further amplified by the presence of the magnetic field [6].

C. Optical Detection Methods

Optical detection methods, employing technologies such as photomultiplier tubes (PMTs) or fluorescent fibers, stand out for their robust isolation from electrical disturbances, ensuring an exceptional immunity to EMI [31]. However, these methods face challenges in detecting internal defects within insulation systems.

Innovative approaches to optical PD detection have demonstrated potential in PD detection under PWM conditions.

Agarwal introduced a nonintrusive PD detection approach using high-speed optical sensors for Kapton polyimide-insulated

TABLE II
SUMMARY OF PD RESEARCH OF MEDIUM TO HFT INSULATION UNDER PWM CONDITIONS

Reference	Device under test (DUT)	Test PWM conditions (max)	PD detection method	Investigated factors	PD characteristics
1 [30]	A back-to-back turn insulation sample, and a single cavity layered insulation	• 4 kHz • 4 kV • Unipolar	• Antenna	• Switching frequency • Overshoot • Rise time	• Max PD magnitude • PD rate
2 [6]	Insulated enamel twisted-pair specimen	• 1 kHz • 2 kV • Bipolar	• Antenna	• Magnetic field	• PDIV • PRPD
3 [26]	Polyimide film	• 1 kHz • 2 kV • Unipolar	• Antenna	• Pressure	• PDIV • PRPD
4 [32]	Kapton polyimide insulated copper foil windings	• 50 kHz • 2 kV • Unipolar	• Optical method	• Switching frequency	• PDIV • PDEV
5 [28]	The twisted Litz wire, and the PCB windings	• 50 kHz • 2.5 kV • Bipolar	• Antenna • HFCT	• dv/dt • Voltage • Switching frequency	• PDIV • PD charge • Number of PD
This paper	**Triple junction (TJ) of winding, insulation, and air**	• **50 kHz** • **4.1 kV** • **Bipolar**	• **Antenna** • **HFCT**	• **Switching frequency** • **Rise time** • **Voltage level** • **Insulation layers**	• **PDIV** • **PRPD** • **PD magnitude** • **PD occurrence time**

copper foil windings in medium-frequency transformers. A PD test platform was developed with unipolar PWM generated by a half-bridge inverter utilizing 3.3 kV SiC devices. Winding samples were tested at PWM voltages up to 2 kV and frequencies up to 50 kHz, with high dv/dt rates reaching 60 V/ns. The study investigated the PD performance, focusing on PDIV and PRPD under different frequencies and dv/dt rates. The results indicate that PDIV and partial discharge extinction voltage (PDEV) are approximately 18% higher when PWM frequencies are below 1 kHz. In addition, the PD characteristics showed negligible dependence on dv/dt in the two test cases [32].

Zang introduced an optical-based PD detection technique that uses fluorescent fibers to achieve electromagnetic and acoustic immunity under single PD pulses. Optical PRPD patterns and PDIV under different air pressure and voltage conditions are investigated. The investigation revealed a proportional relationship between the optical signal and PD amplitude, showing that the severity of PD on PCBs can be effectively detected and evaluated by this method [33].

You et al. employed a combination of a PMT and a 200 MHz bandwidth HFCT to measure PDs. The PD behaviors of direct bonded copper samples with different trench distances and chamfer radii under single and repetitive square pulses with ultrafast dv/dt are studied. The results show that for single pulse excitation, the PDIV decreases with increasing rise time, provided the pulse width is less than a threshold; PDIV also decreases with increasing pulse width, and the PD time delay is increased with increasing pulse width. Based on the test results, an empirical equation for PDIV prediction is developed [34].

D. Other Methods

Other methods, such as acoustic and electrochemical detection, which are based on secondary response detection, have speed limitations that make them less accurate for PD detection under PWM conditions [35], [36].

The above comparison demonstrates the promise of HFCT, UHF antennas, and optical detection methods for PD detection under PWM conditions. Their ability to detect HF signals in the presence of electromagnetic noise positions them as promising tools for effective PD detection.

A summary of recent PD studies relevant to medium to HFT insulation under PWM stress is presented in Table II. While these studies have significantly advanced our understanding of PD behavior in power electronics insulation systems, a critical research gap remains. The PD behavior of TJs in HFTs, identified as the most vulnerable points due to their extreme electrical stress concentration and temperature gradients, has not been comprehensively addressed. Previous research has typically focused on general insulation configurations or specific components such as Litz wires, twisted pairs, PCB windings, or polyimide films, but has not provided a focused investigation of the complex PD phenomena occurring specifically at TJs under high voltage, HF bipolar PWM stress conditions. This gap is particularly significant because the electric field distribution and charge accumulation mechanisms at TJs result in distinctive PD characteristics that directly impact insulation reliability.

This research addresses this critical gap by conducting a systematic investigation of the PD characteristics of TJs in HFTs under bipolar PWM voltage, with particular attention to high voltage and frequency levels relevant to modern power electronics applications. Compared to previous studies, this work develops an experimental platform with enhanced testing capabilities, integrating two different PD detection methods. Furthermore, this study introduces in-depth analysis methods that extend beyond PDIV and PRPD pattern analysis to characterize PD behavior under various PWM conditions. The PD behavior under different PWM conditions and insulation configurations is systematically measured and analyzed, and the underlying mechanisms are thoroughly discussed. The outcomes not only advance theoretical understanding but also offer practical guidance for insulation system design in modern power electronics. The specific contributions of this article are as follows.

1) This article focuses on the PD behavior of the TJ in HFTs under PWM voltage, which has not been thoroughly investigated in previous studies. Based on multiphysics

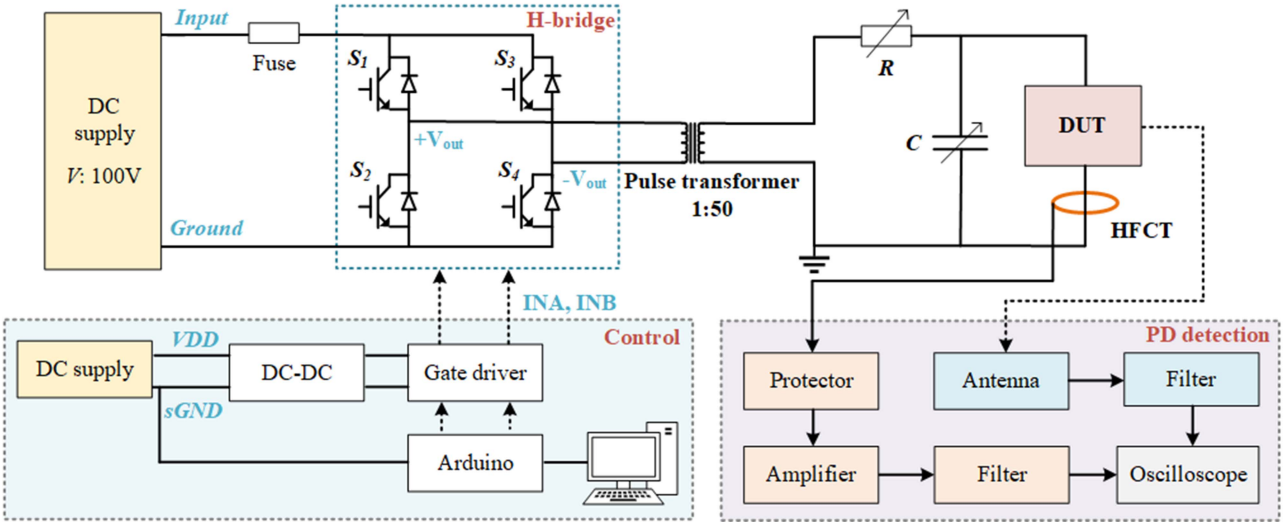

Fig. 2. Topology of PWM voltage PD test platform.

analysis of the HFT [7], the TJ is identified as the point most susceptible to accelerated aging and PD. While previous studies have investigated various insulation configurations, an in-depth investigation specifically targeting this critical weak point in HFTs has not been provided.

2) A high-voltage HF PWM PD test platform is developed, capable of generating PWM voltage up to 10 kV and 50 kHz, enabling the investigation of PD behavior under high voltage PWM conditions relevant to advanced power electronics applications. In addition, a comprehensive review and analysis of the PD detection methods under PWM conditions are performed. Both HFCT and UHF antenna detection methods are employed to provide robust detection of PD signals. This dual-detection approach with theoretical analysis and experimental validation offers valuable reference for PD test setups under PWM stress.
3) A novel approach to analyze PD characteristics under PWM voltage is introduced. Beyond traditional PDIV and PRPD pattern analysis, this study includes a detailed investigation of discharge magnitude and occurrence time characteristics with their corresponding density distributions under various PWM conditions, providing critical insights into the underlying mechanisms of PD under PWM excitations. Furthermore, the effect of multiple factors including switching frequency, rise time, voltage level, and insulation configuration on the PD behavior are systematically investigated in this research.

The rest of this article is organized as follows. Section II introduces the PWM voltage PD test platform for the HFT insulation. Section III covers the PD mechanism at TJ under PWM stress. Section IV presents the PD test results and analyzes the PD behavior under various PWM conditions. Finally, Section V concludes this article.

II. PWM Voltage PD Test Platform

To investigate the PD behavior of the HFT insulation under high-voltage PWM stress, a PWM voltage PD test platform is designed and developed. The topology of the PD test platform is illustrated in Fig. 2, including a high-voltage PWM generator, device under test (DUT), and PD detection equipment.

TABLE III
Parameters of the Pulse Transformer

Specification	Value/range
Primary side	230 V
Secondary side	10 kV
Turns ratio	1:50
Frequency range	10-50 kHz

A. High-Voltage PWM Generator and Typical Waveform

The high-voltage PWM generator consists of a full-bridge inverter with a high-voltage dc source, an HF pulse transformer, high-voltage resistors, and capacitors [37]. The full-bridge inverter is controlled by Arduino and generates a low-voltage PWM waveform.

The voltage waveform is transformed into high voltage by an HF pulse transformer with a turn ratio of 1:50. The electrical parameters of the pulse transformer are provided in Table III [38]. The pulse transformer uses an N87 MnZn ferrite U-core from TDK for the magnetic core. The primary windings are made of 3 mm thick silicon-insulated wire, while the secondary high-voltage winding is constructed with a 200-turn enameled wire. The low-voltage winding is placed inside the high-voltage winding, and both bobbins are printed in polylactic acid. The prototype of the pulse transformer is shown in Fig. 3. A detailed design process and experiment validation can be found in [38] and [39].

The rise time of the PWM voltage is adjusted using RC elements, including an adjustable high-voltage resistor bank and an adjustable capacitor. By varying the values of the resistance and capacitance in the circuit, the output PWM pulse waveform could be tuned, allowing for the testing of DUTs under different rise times.

The PWM voltage generator is capable of producing PWM pulses with a maximum voltage of up to 10 kV, a frequency

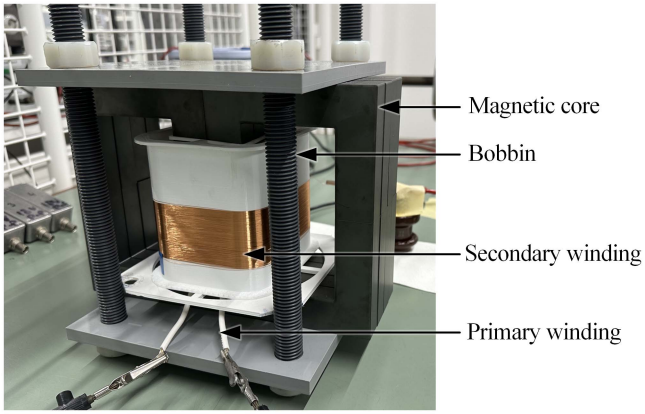

Fig. 3. Prototype of the pulse transformer.

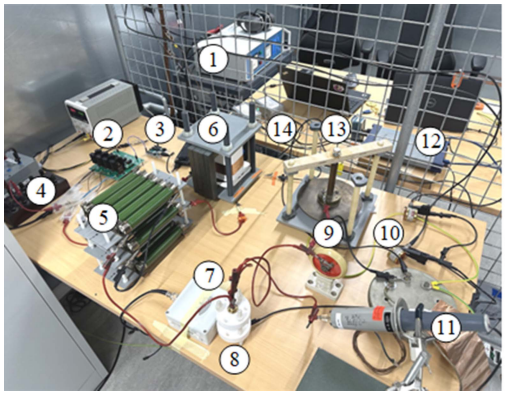

Fig. 4. Physical realization of the test platform.

TABLE IV
EQUIPMENT MODEL AND PARAMETERS

Equipment	Model	Parameter
DC supply (control)	BASE BT-305	0-30 V
DC supply (H-bridge)	Hp 6477C 0-250V	0-250 V
HFCT	Begoz FCT-016-5.0	2 kHz-1 GHz
UHF antenna	TECHMP 045TMH20-20A018	400 Mhz-3 GHz
High pass Filter	Mini-circuits 15542	500 MHz
Control board	Arduino UNO R3	-
Oscilloscope	Picoscope 6404C	-
High voltage probe	TEKTRONIX	0-20 kV

range of up to 50 kHz, and a rise time range of 3.5–10 μs. The physical look of the PD test platform is present in Fig. 4. The model and parameters of the main equipment used to develop the test platform are given in Table IV. A typical waveform with a PWM voltage amplitude of 1.2 kV, a frequency of 10 kHz, and a rise time of 3.5 μs is shown in Fig. 5.

The platform was tested up to 5 kV within a frequency range of 10–50 kHz without the test samples, and no discharges were detected using HFCT and UHF antennas. The test results confirm that the test platform is PD-free under the tested conditions.

B. PD Detection Methods

In general, PD signals occurred near a zero crossing or near the peak voltage of falling and rising edge under PWM

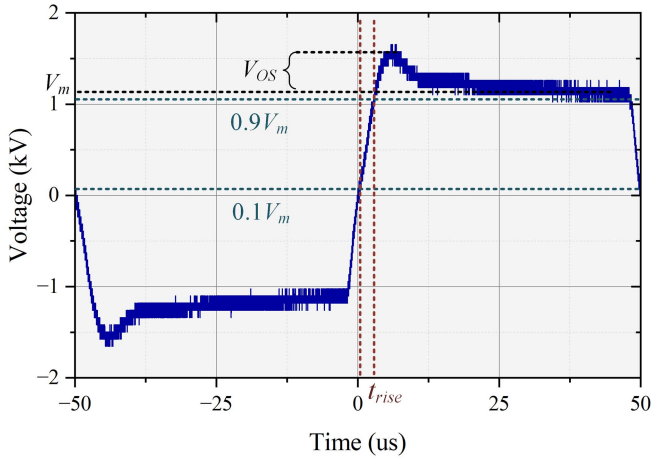

Fig. 5. Typical PWM waveform with a voltage amplitude of 1.2 kV, a frequency of 10 kHz, and a rise time of 3.5 μs (V_m represents the voltage amplitude, t_{rise} represents the rise time, and V_{os} represents the overshoot).

excitations [28]. This raises the challenge of differentiating PD occurring in the vicinity of the rising and falling edges from commutation/switching noise. This interference overlaps with PD signals in both the time and frequency domains, complicating PD measurements under such conditions.

It has been reported that both PD and switching disturbances exhibit significant energy distribution below 500 MHz. However, PD pulses generated by impulse voltages with shorter rise times tend to distribute their energy above 500 MHz, with an upper limit of around 2 GHz [16], [26]. To address this, the sensors used for PD testing under impulsive voltages need to have a wide frequency response. In addition, high-pass filters are necessary to further improve interference rejection.

A schematic representation of the possible overlap between the voltage impulse and PD pulse frequency spectra is shown in Fig. 6 [40]. After filtering, the HF energy from the PD pulses is retained, while the low-frequency energy generated by both PD and disturbances is removed. The cut-off frequency of a filter is critical in ensuring that after filtering the PD signal magnitude exceeds that of the voltage impulse within the PD detector's bandwidth.

To improve the accuracy and reliability of PD signal measurements, both HFCT and UHF antennas are used for PD signal detection. The UHF antenna has a bandwidth of 500 MHz to 2.5 GHz and is connected to a high-pass filter with a cutoff frequency of 400 MHz. HFCT has a bandwidth of 2 kHz to 1 GHz and is connected to a high-pass filter with a cutoff frequency of 100 MHz to enhance measurement reliability. The accuracy and effectiveness of the detection methods will be discussed in Section III-B.

Since the apparent magnitude of PD is related to the distance between the UHF antenna and the DUT, the relative positions of the antenna and the DUT are kept constant throughout the tests [23]. PD measurements of each DUT are repeated six times under each condition to obtain a statistical distribution. The time interval between each test is longer than 10 min to minimize the influence of residual space charge from the previous test [28].

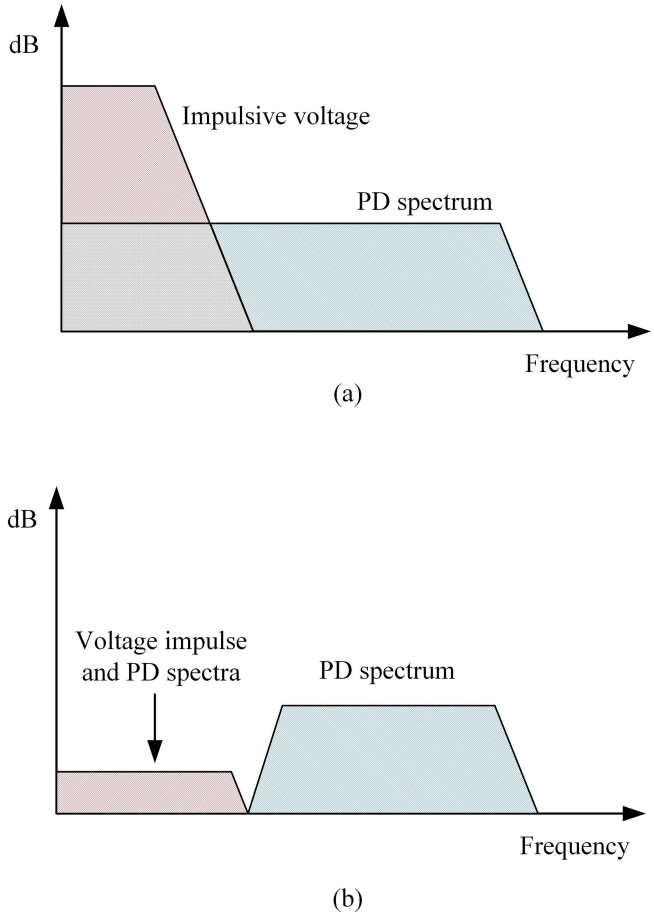

Fig. 6. Energy distribution of voltage impulse and PD. (a) Overlap between voltage impulse and PD pulse spectra. (b) Voltage impulse and PD pulse spectra after filtering [40].

TABLE V
SELECTED LEVELS FOR EACH FACTOR

Level	Rise time (μs)	Frequency (kHz)	Voltage (kV)
Low	3.5	10	3.2
Medium	6	35	3.6
High	9.5	50	4.1

C. DUT and Investigated PWM Parameters

To replicate the electrical stress subjected to the TJ of the HFT, the electrodes are designed into two cylinders with chamfered edges, with the DUT securely placed between them [10]. DUT is the insulation paper (Nomex 410), which is widely used as the main insulation of the HFT. Stainless steel is used for the electrodes and the surface is finely polished. The electrode structure is shown in Fig. 7.

The investigation of PD behavior focuses on three critical parameters: PWM voltage magnitude, rise time, and PWM frequency. The values of these parameters are carefully selected based on the insulation capability and working conditions of DUT. The selected values of each parameter are given in Table V. To achieve an effective comparison, all other test parameters remain constant when any of the factors above are varied.

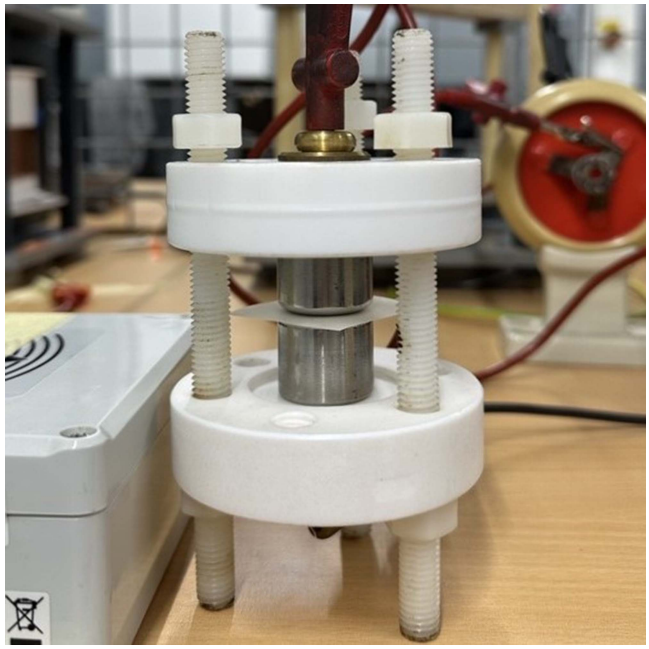

Fig. 7. Electrodes with the DUT.

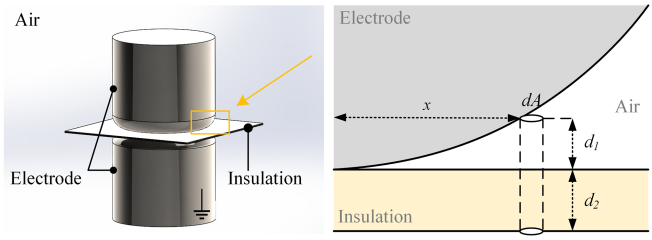

Fig. 8. Schematic diagram of the TJ.

III. PD MECHANISM UNDER PWM STRESS

A. PD Mechanism at TJ

Solid insulation used to support conductors at high voltages induces TJs—regions where metal, solid insulation, and gas are in contact [41]. These junctions are identified as weak points within the insulation system, largely due to the discrepancy in permittivity between the solid and gas.

Fig. 8 shows a simplified model of a TJ, consisting of air, electrodes, and insulation, to facilitate the understanding of PD phenomena. By considering a cylindrical volume with an end area dA located at a distance x from where the electrodes and insulation meet, the electric field within this volume is assumed to be uniform vertically for sufficiently small. When a voltage V is applied across the electrodes, a voltage V_1 is induced across the air gap, as described in [8]

$$V_1 = \frac{V d_1}{d_1 + \left(\frac{\varepsilon_1}{\varepsilon_2}\right) d_2} \tag{1}$$

where d_1 and d_2 are the thickness of the air gap and insulation, respectively, and ε_1 and ε_2 are their corresponding permittivities. The stress in the air gap will exceed that of the solid by the ratio of permittivities. The stress in the air gap increases further as x

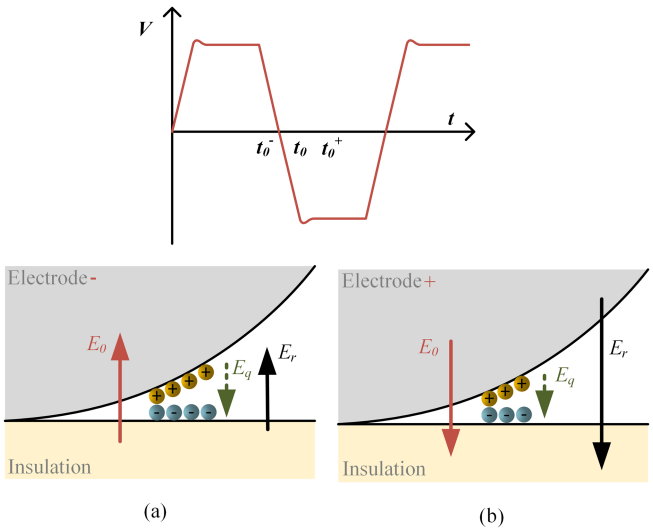

Fig. 9. Electric field distribution before and after voltage polarity reversal without occurring of PD. (a) $t = t_0^-$, E_0 is in the opposite direction to E_q. (b) $t = t_0^+$, E_0 is in the same direction as E_q.

is decreased, and reaches very high values as d_1 becomes very small, leading to the air breaking down at a relatively low applied voltage.

The charge at the tip of the discharge will further disturb the applied local field and transform the arrangement into a highly nonuniform system [42]. The charge concentration at the tip of a discharge channel might be sufficient to give a local field of several megavolts per centimeter [43]. If the design of these regions is not carried out with great care, PDs may appear and accelerate the aging of the insulation.

A PD event is initiated when the following two basic conditions are met [44].

1) A starting electron is available.
2) The local field is sufficiently high to generate an avalanche from the free electron.

While the second condition is deterministically influenced by the applied electric field, other stresses, and the geometry and electrical characteristics of the system, the first condition typically occurs at random [45]. This highlights the inherent stochastic nature of PD, which is reflected in their variable amplitude and occurrence time.

The distribution of the electric field at TJ depends not only on the applied voltage but also on the presence of space charge [46]. As illustrated in Fig. 9, when a PD occurs, a charge transfer happens in the air gap. Positive and negative charges will be deposited on surfaces. The space charge deposited by an avalanche reduces the external field, allowing for the extinction of the PD event [47]. After a half cycle when $t = t_0$, the applied voltage starts decreasing and changing the polarity. However, the induced field E_q by the surface charge will remain longer due to the longer relaxation time of surface charges, and it will enhance the electric field during the falling edge, as shown in Fig. 9(b) [28].

The space charge decay time constant is associated with the charge drift and recombination rates [48], [49], [50]. The range of charge decay times reported in [28] and [51] are on the millisecond level. Given that the applied PWM frequency in this study is between 10 and 50 kHz, the charge decay time can be much longer than the voltage impulse duration. Therefore, under fast PWM conditions, E_q does not fully decay between voltage cycles, influencing subsequent electric fields and PD behavior. The persistent E_q needs to be considered when analyzing PD mechanisms under HF PWM excitation.

B. Typical Waveforms of PD

Fig. 10 demonstrates PWM waveform along with the typical PD signals captured by both the HFCT and UHF antenna. The waveforms are recorded with an applied voltage of 1.2 kV, a frequency of 10 kHz, and a rise time of 3.5 μs to compare the effectiveness of each method in detecting PD under PWM conditions. The figure presents the global waveforms of the first and second PD events, along with zoomed-in views of each PD signal for detailed analysis.

The test results from the UHF antenna indicate that the PD signal magnitude significantly exceeds the voltage impulse magnitude within the PD detector's bandwidth, allowing us to accurately detect PD signals. While the HFCT uses a high-pass filter with a lower cutoff frequency, some interference remains. During both the rising and falling edges, repetitive commutation noise is observed at the start of the switching time, as detected by the HFCT, with the PD signal superimposed on the interference. Nevertheless, the detection results from both the UHF antenna and the HFCT are consistent, verifying the accuracy of the measurement method.

The first PD occurs when the voltage reaches it is peak value. Notably, most PDs occur on the rising or falling edge of the PWM voltage, rather than during the voltage plateau phase. To explain this phenomenon, the PD process is analyzed in two cases when the voltage is on the rising edge as in the example shown in Fig. 11.

1) Case 1: The External Electric Field E_0 is in the Opposite Direction to the Local Electric Field E_q: In this case, the local electric field E_q induced by accumulated discharge reduces the external electric field E_0 when PD occurs. At $t = t_1$, PD happens at the TJ, leading to charge transfer and the dissipation of the charge avalanche associated with the PD event, as shown in Fig. 11(a).

After the PD event when t reaches t_1^+, the local electric field E_q approaches zero, while the residual field E_r is almost equal to the external field as depicted in Fig. 11(b). At this point, under the effect of the external field, the movement of space charges tends to build up the local electric field that reduces the external field. The directions of the space charges are denoted with D^- and D^+ in the figure. When the external field becomes high enough again, another PD event may occur.

When the voltage reaches the plateau phase at $t = t_2$, as shown in Fig. 11(c), the external field no longer increases. Meanwhile, the local electric field continues to build up and further decreases the external field, thus reducing the possibility of PD occurrences at this stage.

2) Case 2: The External Electric Field E_0 is in the Same Direction as the Local Electric Field E_q: In this case, the local electric field enhances the external field when PD occurs, as shown in Fig. 11(d). At $t = t_1$, PD happens, leading to charge transfer at TJ.

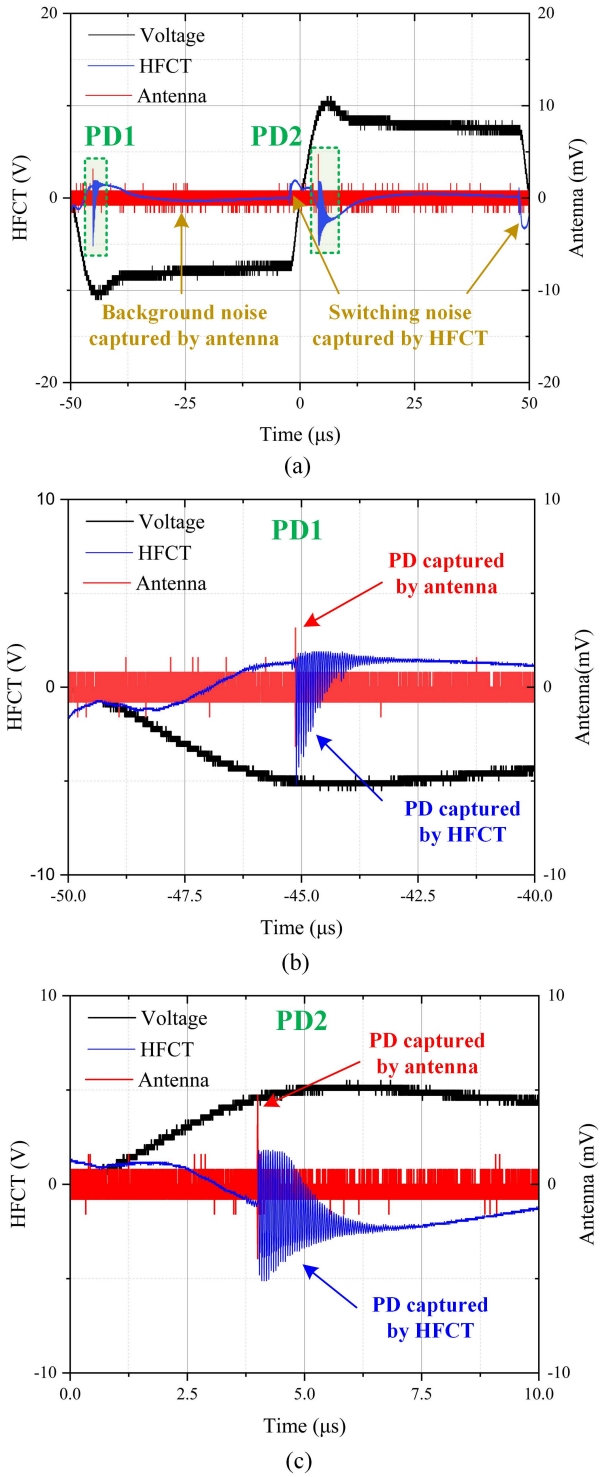

Fig. 10. Typical waveforms of PD. (a) Global waveforms. (b) Zoom-in waveforms of the first PD. (c) Zoom-in waveforms of the second PD.

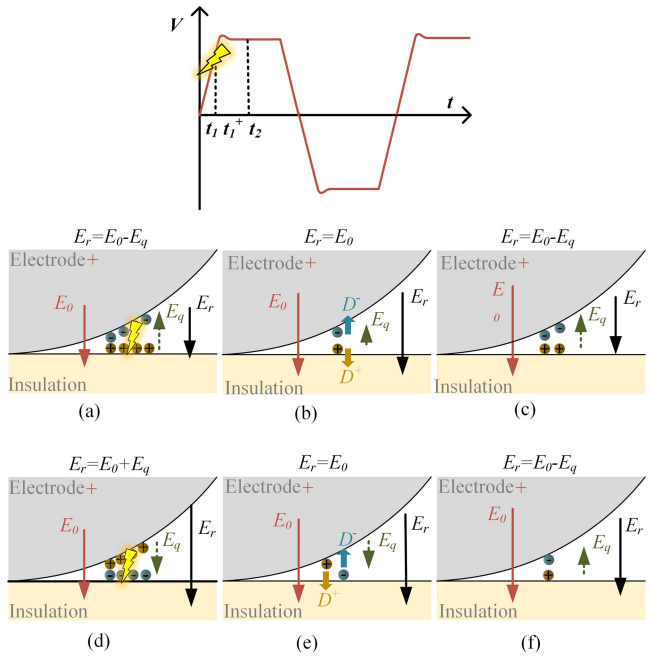

Fig. 11. Electric field distribution during the PD process.

After the PD event, the residual electric field approaches the external field, while the residual local electric is close to zero, as illustrated in Fig. 11(e). The movement of space charges now acts to reduce the external electric field, causing the local electric field to weaken the external field. As the externally applied voltage reaches the plateau period at $t = t_2$, as shown in Fig. 11(f), the external electric field no longer increases, and the internal electric field continues to weaken it. This results in PD events that predominantly occur during the rising edge of the voltage waveform.

In summary, the difference between the two cases is whether the electric field generated by the accumulated space charge is in the same or opposite direction to the external electric field during the PD event. In either case, after a PD occurs, the local electric field approaches zero, and the total electric field becomes approximately equal to the external field. As space charge accumulates after PD, it always acts to weaken the external field. Specifically, in Case 1, where the initial local field opposes the external field, charge accumulation further weakens the external field. In Case 2, where the initial local field enhances the external field, the accumulation process tends to reduce this enhancement and may eventually reverse to weaken the external field. Both cases will be considered when analyzing the PD behaviors to interpret the experimental phenomena in the subsequent section.

IV. Test Results and PD Behavior Under PWM Voltage

The PD characteristics of RPDIV and PRPD patterns are analyzed with different conditions of PWM frequency, rise time, and voltage when the DUT is three layers of insulation. RPDIV, is defined as the voltage level at which at least five PD occurs in ten voltage impulses.

A. PD Characteristics Under Different PWM Frequencies

Fig. 12 shows the correlation between PWM frequency and RPDIV at a constant rise time of 3.5 μs. The connecting line is the mean of the RPDIV results for each test condition. As the frequency increases, the RPDIV increases. This can be explained by the frequency dependence of the insulation material. In the

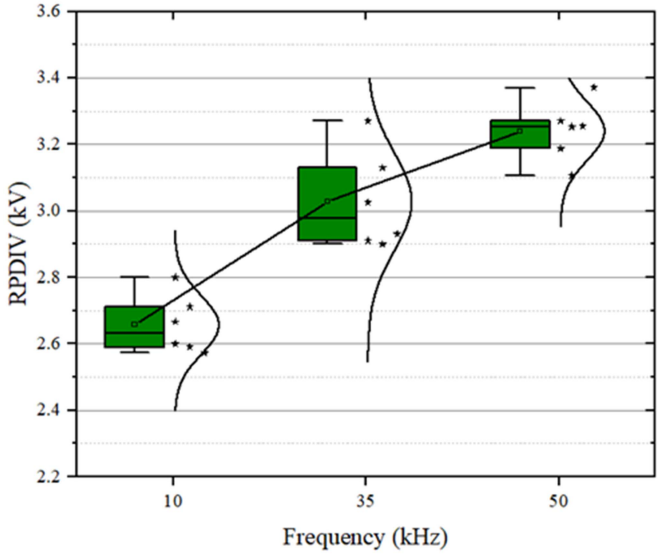

Fig. 12. Relationship between PWM frequency and RPDIV.

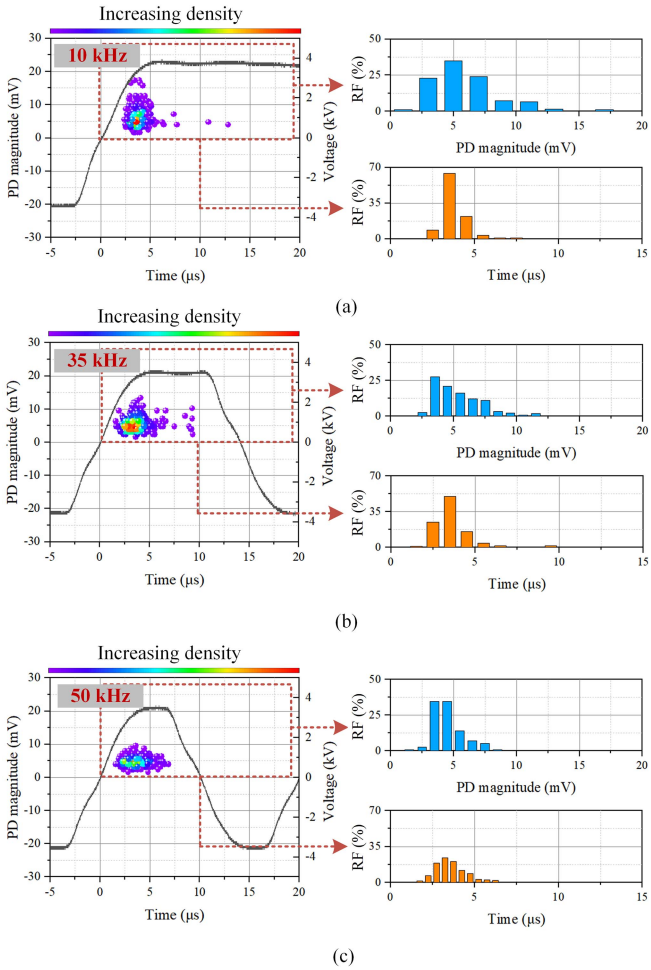

Fig. 13. PRPD patterns at different PWM frequencies. (a) 10 kHz. (b) 35 kHz. (c) 50 kHz.

frequency range of 10–50 kHz, the dielectric constant of the insulation paper tends to decrease with increasing frequency [52]. As shown in (1), a decrease in the dielectric constant results in a decrease in the maximum electric field at the TJ, thus requiring a higher voltage to initiate PD.

The PRPD patterns at different PWM frequencies when the voltage amplitude is 3.5 kV and the rise time is 3.5 μs at the rising edge are shown in Fig. 13. PRPD plots capture the timing and magnitude of PDs relative to the voltage waveform. Here, $t = 0$ is defined as the point at which the voltage is zero. To visualize the PRPD patterns under different operating conditions, the histograms of the relative frequency (RF) distribution of PD occurrence time and discharge magnitude are analyzed and displayed to the right of the density plot.

With an increase in frequency, a noticeable concentration in both the magnitude and the occurrence time of PD events is observed. This phenomenon could be explained as the switching frequency increases, the time available for space charge accumulation within each half voltage cycle is reduced. Consequently, the magnitude of the local electric field generated by space charge accumulation is reduced, regardless of whether it initially weakens or enhances the external electric field, leading to a smaller overall influence on the total electric field as the switching frequency increases.

Based on the mechanism analysis of PD under PWM voltage discussed in Section III, the local electric field generated by space charge accumulation influences the total electric field, thereby affecting both the occurrence timing and magnitude of PD. When the local field initially opposes and weakens the external field (as described in Case 1, Section III), the extent of this weakening is reduced at higher frequencies due to the limited accumulation of space charge. When the local field initially enhances the external field (as in Case 2), the enhancement effect also diminishes as frequency increases. In both cases, the total electric field is less affected by the space charge accumulation, causing the PD occurrence timing and discharge magnitudes to become more concentrated. The constancy of the highest density region in the PRPD plots underlines the predominant influence of the applied voltage on the PD behavior.

Another observation is the increased occurrence of PDs during the plateau phase of the voltage as the frequency rises. At higher frequencies, surface charges at the TJ may not fully stabilize or redistribute before the next pulse of applied voltage. This incomplete recovery leads to dynamic field distortions during the plateau phase, resulting in an increased occurrence of PD events during this stage. However, the majority of PDs still occur during the rising phase because the external electric field remains the dominant factor driving PD behavior.

B. PD Characteristics at Different Rise Times.

When the frequency is 10 kHz, the relationship between rise time and RPDIV is shown in Fig. 14, where RPDIV increases as the rise time increases. This can be explained by two scenarios.

The local electric field generated by space charge accumulation can either enhance or weaken the external electric field, depending on their relative directions. When the external and local fields are in opposite directions, the local field weakens the external field, reducing the possibility of PDs. However, PDIV is determined by the strongest total electric field, which occurs when the local and external fields are in the same direction. In

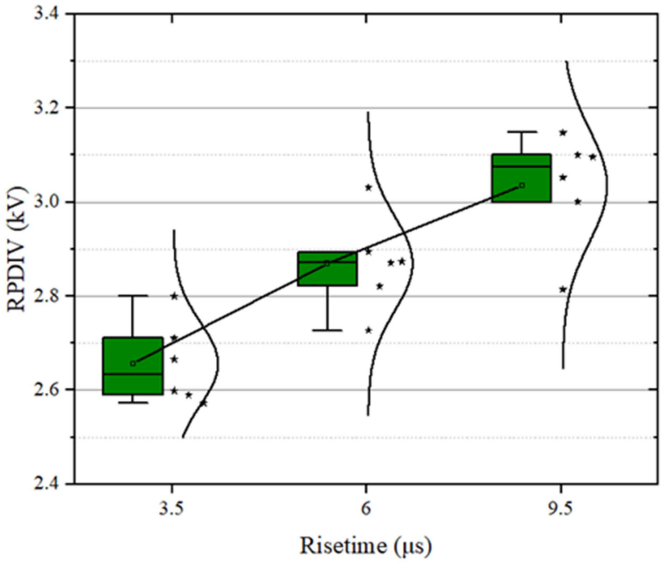

Fig. 14. Relationship between rise time and RPDIV.

this case, the local field strengthens the external field. A shorter rise time reduces the time available for space charge recombination and dissipation, leading to a stronger enhancement of the external field and an increase in PDIV as the rise time increases.

For a frequency of 10 kHz and a voltage level of 3.3 kV, the PRPD plots for different rise times are shown in Fig. 15. A notable observation is the concentration of the PD amplitude range as the rise time increases. At the same time, the occurrence time of the PD shows a clear trend toward delay.

To further investigate the influence of rise time on the timing of PD occurrence, the timing of PD occurrence is normalized, meaning that the time of occurrence of PDs is divided by their rise time. The PRPD plot of the normalized time on the x-axis after processing is shown in Fig. 16. As the rise time increases, the normalized time of PD occurrence does not change significantly. However, the time range of the normalized time shows a significant trend to narrow.

One possible explanation for these patterns is the impact of the local electric field induced by the space charge accumulation. As the rise time increases, the rate at which the external voltage changes slows down, allowing more time for space charge dissipation and recombination before the voltage reaches its peak. This results in a weaker local electric field from accumulated charges, regardless of whether it initially weakens or enhances the external electric field. In both cases discussed in Section III, the total electric field is less influenced by space charge effects, leading to a more uniform PD occurrence and magnitude distribution.

In addition, as the rise time increases, there is a longer delay in reaching equivalent electric field strengths, resulting in a rightward shift of PD occurrence times on the x-coordinate axis in Fig. 15, while no significant change in normalized time is observed in Fig. 16. This characteristic in the time occurrence of PD illustrates a concentration of PD events around times when the applied voltage is approaching its peak. This trend highlights the direct effect of rise time on PRPD characteristics and

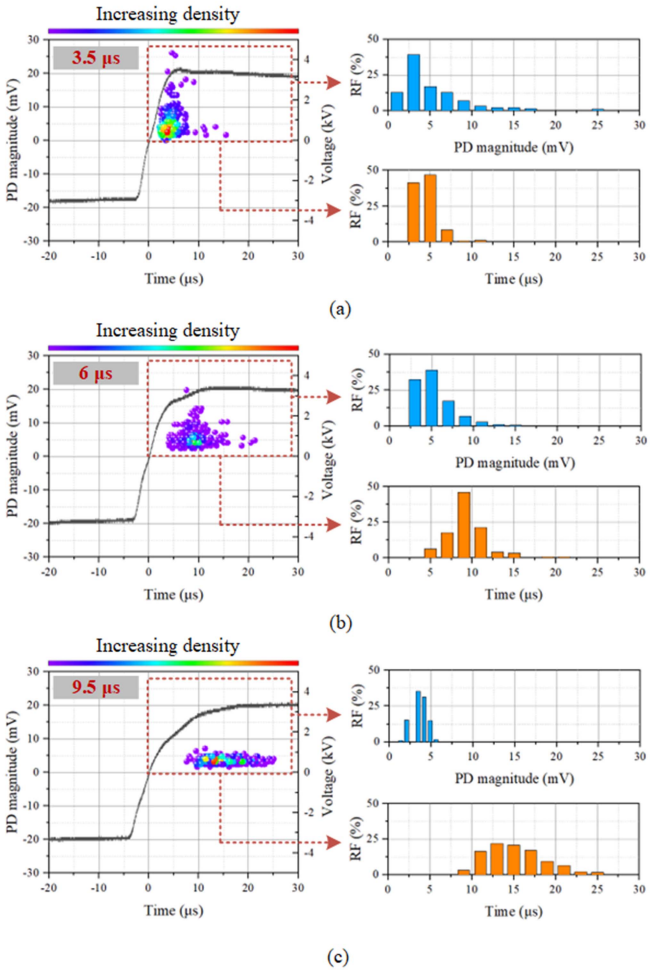

Fig. 15. PRPD patterns at different rise times. (a) 3.5 μs. (b) 6 μs. (c) 9.5 μs.

underlines the critical role of rise time in determining the timing and probability of PD events near peak voltage conditions.

However, it is important to acknowledge that the observed differences in PD behavior may not be solely attributed to the rise time. While the analysis suggests that rise time may influence PD characteristics through its effect on space charge accumulation, other aspects of the waveform, including overshoot voltage, may also contribute to the observed trends. Notably, decreasing the rise time (increasing the slew rate), depending on the circuit's impedance, can lead to a higher overshoot even when the voltage amplitude remains constant, introducing additional voltage stresses on the turn insulation and TJs [53], [54]. Recent studies have shown that overshoot can significantly impact PD behavior and interacts with other factors, including rise time, frequency, and voltage level [30], [55], [56]. Therefore, other factors such as overshoot, along with the complex interactions between various influencing factors, may also play a role in the observed PD behavior.

In the future, we will further investigate the influence of overshoot on PD behavior and its interactions with other factors through the design of experiment method, which may provide additional insights into the contributing effects influencing PD characteristics in HFT insulation systems.

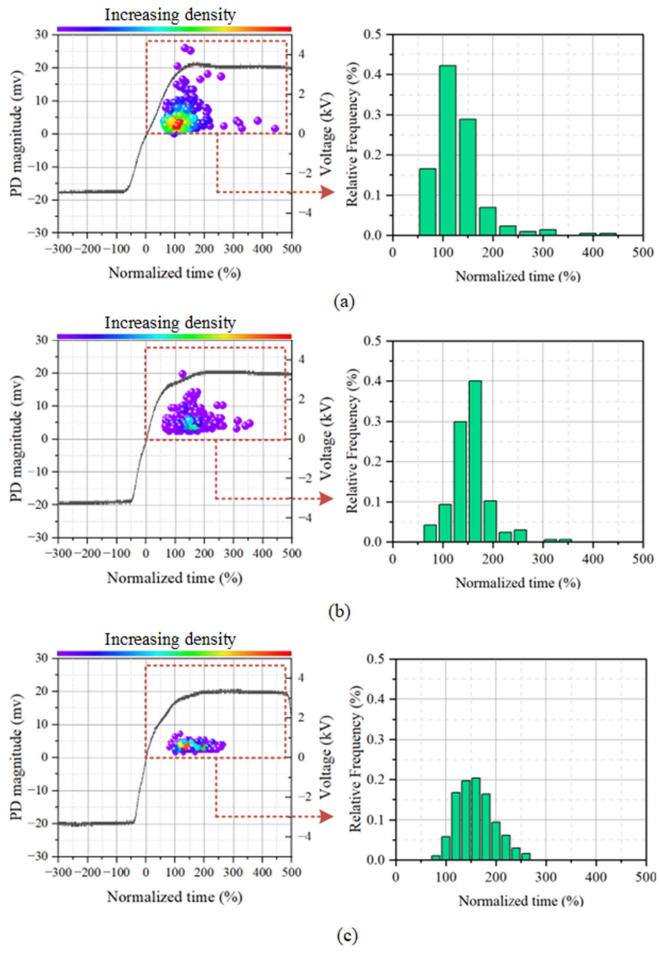

Fig. 16. PRPD patterns at different rise times with normalized times. (a) 3.5 μs. (b) 6 μs. (c) 9.5 μs.

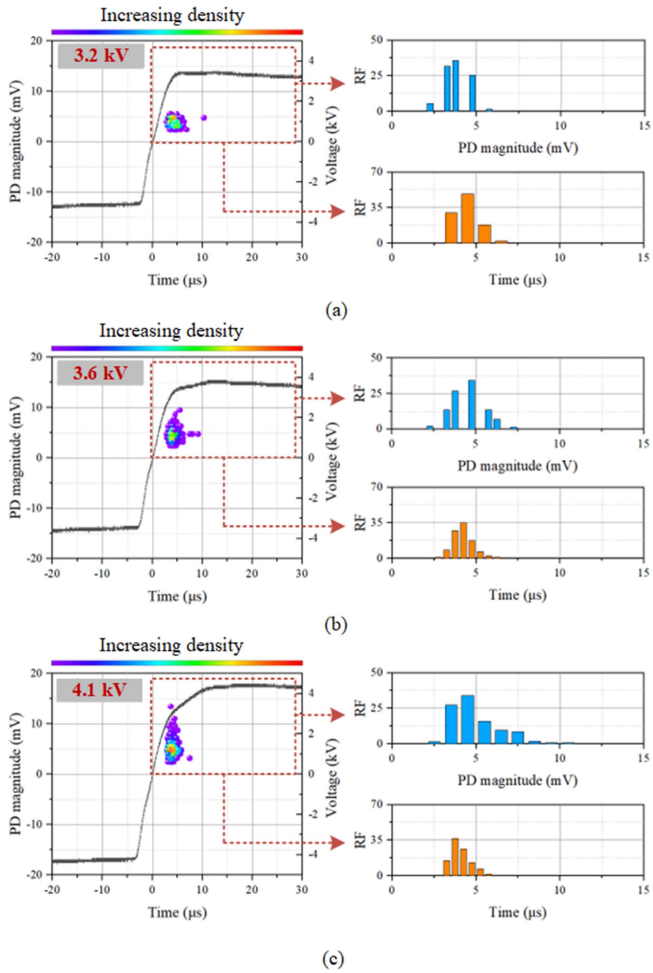

Fig. 17. PRPD patterns at different voltage levels. (a) 3.2 kV. (b) 3.6 kV. (c) 4.1 kV.

C. PD Characteristics at Different Voltage Levels

The PRPD plots at different voltages with a frequency of 10 kHz and a rise time of 3.5 μs are shown in Fig. 17. It is observed that an increase in voltage leads to a broader range of PD magnitudes and higher discharge levels. The time range of PD occurrence and the position of the highest density on the plot did not change significantly.

In summary, a significant correlation is found between RPDIV and both PWM frequency and rise time. The density distribution of PD magnitude is influenced by a combination of factors: frequency, rise time, and voltage level. In addition, the time of occurrence of PDs is primarily influenced by frequency and rise time, while rise time has a critical influence on the time when PDs are most likely to occur. These characteristics can be attributed to the complex interaction of factors under HF PWM pulses, including the applied voltage level, the internal field induced by space charges, and the geometry of the TJ, in addition to the PWM frequency and rise time. These observations are consistent with the mechanism analysis revealing that the characteristics of PDs under HF PWM conditions are significantly influenced by both the external and local electric fields. The external field is determined by the amplitude of the

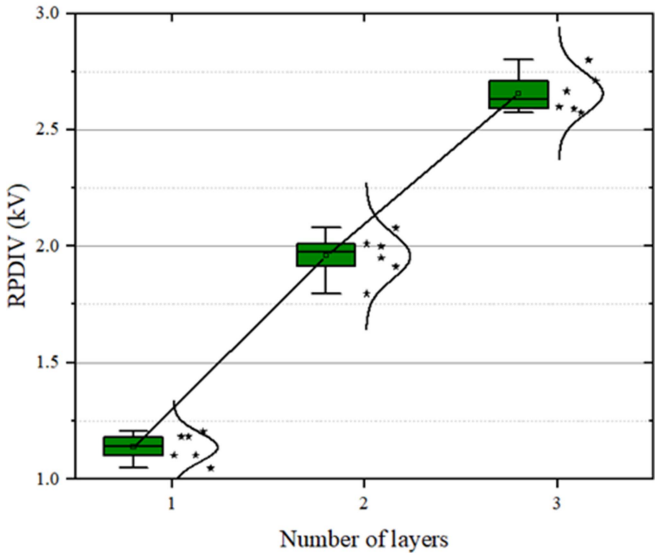

Fig. 18. Relationship between RPDIV and number of insulation layers.

applied voltage, while the local field is a consequence of space charge accumulation. In particular, the strength of the local electric field is closely related to the frequency and rise time of the PWM voltage.

D. Influence of the Number of Layers

To study the influence of the number of insulation layers on the PD behavior, experiments are carried out when the insulation paper is 1, 2, and 3 layers, respectively. Fig. 18 shows the relationship between the number of insulation layers and the RPDIV. A nearly linear increase in RPDIV is observed with an increase in the number of insulation layers. This pattern suggests that systematically increasing the insulation layers improves the insulation system's ability to withstand PD, effectively improving the reliability of the HFT.

V. Conclusion

The performance and reliability of electrical insulation subjected to fast-switching PWM-modulated excitation is a critical concern in several areas, including power grids, industry, and transportation. This article investigates the PD behavior of HFT insulation under high-voltage PWM stress. A high-voltage, HF PWM PD test platform designed for HFT insulation is developed. An antenna and an HFCT with filters are set up to effectively detect PD signals under PWM conditions. The test results show that the RPDIV increases with increasing frequency, rise time, and the number of insulation paper layers for PWM voltages in the frequency range of 10–50 kHz. The PRPD characteristics are related to the frequency, rise time, and voltage level of the applied voltage, exhibiting different distribution patterns under various conditions. These patterns are observed in the timing of partial discharge occurrences, the amplitude of discharges, the distribution of RF, and the location of the highest density position of PDs. An in-depth study of the PD mechanisms under PWM voltage is performed, providing insights that explain the observed test results.

The results of this study are critical to improving the understanding of insulation performance under PWM stress. Knowledge of the PDIV is key to predicting when PDs are likely to occur, which supports the development of accurate lifetime models for insulation in both PD and non-PD scenarios. Insight into the nature of PRPD behavior and the factors influencing PD activity is valuable in assessing insulation aging and degradation. By considering PD at critical regions like the TJ, it is possible to achieve a PD-free insulation system, enhancing the life and reliability of HFTs. Future research will focus on exploring the influence of overshoot on PD behavior and the interactions between different factors through the design of experimental methods, and conducting space charge distribution measurements using pulsed electro-acoustic methods and finite element method modeling to further reveal the mechanisms governing PD behavior under PWM excitation.

References

[1] X. She, A. Q. Huang, and R. Burgos, "Review of solid-state transformer technologies and their application in power distribution systems," *IEEE Trans. Emerg. Sel. Topics Power Electron.*, vol. 1, no. 3, pp. 186–198, Sep. 2013.

[2] Z. Li, E. Hsieh, Q. Li, and F. C. Lee, "High-frequency transformer design with medium-voltage insulation for resonant converter in solid-state transformer," *IEEE Trans. Power Electron.*, vol. 38, no. 8, pp. 9917–9932, Aug. 2023.

[3] E. Serban, C. Pondiche, and M. Ordonez, "Analysis and design of bidirectional parallel-series dab-based converter," *IEEE Trans. Power Electron.*, vol. 38, no. 8, pp. 10370–10382, Aug. 2023.

[4] Z. Yi, K. Sun, H. Liu, G. Cao, and S. Lu, "Design and optimization of the insulation of medium-voltage medium-frequency transformers for solid-state transformers," *IEEE Trans. Emerg. Sel. Topics Power Electron.*, vol. 10, no. 4, pp. 3561–3570, Aug. 2022.

[5] Z. Guo et al., "A novel high insulation 100 kW medium frequency transformer," *IEEE Trans. Power Electron.*, vol. 38, no. 1, pp. 112–117, Jan. 2023.

[6] M. Florkowski, "Magnetic field effects on partial discharges in electrical insulation subjected to PWM excitation," *IEEE Trans. Power Electron.*, vol. 39, no. 2, pp. 2741–2750, Feb. 2024.

[7] Z. Wang, C. L. Bak, H. Wang, H. Sørensen, and F. F. da Silva, "Multiphysics digital model of the high frequency transformer for power electronics application considering electro-thermal interactions," *IEEE Trans. Power Electron.*, vol. 38, no. 11, pp. 14345–14359, Nov. 2023.

[8] J. Kuffel and P. Kuffel, *High Voltage Engineering Fundamentals*. Amsterdam, The Netherlands: Elsevier, 2000.

[9] T. Takuma and T. Kawamoto, "Field enhancement at a triple junction in arrangements consisting of three media," *IEEE Trans. Dielectr. Electr. Insul.*, vol. 14, no. 3, pp. 566–571, Jun. 2007.

[10] Z. Wang, F. F. da Silva, H. Sørensen, Q. Wang, and C. L. Bak, "The interactions analysis for high frequency transformers insulation under multi-stress of high voltage, high frequency, and high temperature," in *Proc. IEEE 2nd Int. Power Electron. Appl. Symp.*, 2023, pp. 734–738.

[11] W. Wang et al., "An improved design procedure for a 10 kHz, 10 kW medium-frequency transformer considering insulation breakdown strength and structure optimization," *IEEE Trans. Emerg. Sel. Topics Power Electron.*, vol. 10, no. 4, pp. 3525–3540, Aug. 2022.

[12] Y. Cao, K. Ngo, and D. Dong, "A scalable electronic-embedded transformer, a new concept toward ultra-high-frequency high-power transformer in dc–dc converters," *IEEE Trans. Power Electron.*, vol. 38, no. 8, pp. 9278–9293, Aug. 2023.

[13] M. Mogorovic and D. Dujic, "100 kW, 10 kHz medium-frequency transformer design optimization and experimental verification," *IEEE Trans. Power Electron.*, vol. 34, no. 2, pp. 1696–1708, Feb. 2019.

[14] E. L. Barrios, A. Urtasun, A. Ursúa, L. Marroyo, and P. Sanchis, "High-frequency power transformers with foil windings: Maximum interleaving and optimal design," *IEEE Trans. Power Electron.*, vol. 30, no. 10, pp. 5712–5723, Oct. 2015.

[15] W. Shen, F. Wang, D. Boroyevich, and C. W. Tipton IV, "High-density nanocrystalline core transformer for high-power high-frequency resonant converter," *IEEE Trans. Ind. Appl.*, vol. 44, no. 1, pp. 213–222, Jan./Feb. 2008.

[16] W. Zhou, P. Wang, Z. Zhao, Q. Wu, and A. Cavallini, "Design of an archimedes spiral antenna for pd tests under repetitive impulsive voltages with fast rise times," *IEEE Trans. Dielectr. Electr. Insul.*, vol. 26, no. 2, pp. 423–430, Apr. 2019.

[17] X. Wang, B. Li, H. Roman, O. Russo, K. Chin, and K. Farmer, "Acousto-optical pd detection for transformers," *IEEE Trans. Power Del.*, vol. 21, no. 3, pp. 1068–1073, Jul. 2006.

[18] *High-Voltage Test Techniques: Partial Discharge Measurements*, International Electrotechnical Commission Standard IEC-60270, 2000.

[19] A. Rodrigo, P. Llovera, V. Fuster, and A. Quijano, "Influence of high frequency current transformers bandwidth on charge evaluation in partial discharge measurements," *IEEE Trans. Dielectr. Electr. Insul.*, vol. 18, no. 5, pp. 1798–1802, Oct. 2011.

[20] Y. Zang et al., "Partial discharge behavior of typical defects in power equipment under multilevel staircase voltage," *IEEE Trans. Dielectr. Electr. Insul.*, vol. 29, no. 4, pp. 1563–1573, Aug. 2022.

[21] O. Šefl, R. Färber, and C. M. Franck, "On the frequency dependence of the PDIV in twisted pair magnet wire analogy in dry air," *IEEE Trans. Dielectr. Electr. Insul.*, vol. 30, no. 5, pp. 2378–2385, Oct. 2023.

[22] K. Liu et al., "The physical mechanism of frequency-induced inflection point for oil–paper insulation under high-frequency square-wave voltage," *IEEE Plasma Sci.*, vol. 50, no. 8, pp. 2388–2395, Aug. 2022.

[23] X. Liu et al., "Characteristics and identification of partial discharge for insulation structures in high voltage IGBT modules under positive square wave voltage," *IEEE Trans. Power Electron.*, vol. 38, no. 4, pp. 5347–5359, Apr. 2023.

[24] J. Li, T. Jiang, C. Cheng, and C. Wang, "Hilbert fractal antenna for UHF detection of partial discharges in transformers," *IEEE Trans. Dielectr. Electr. Insul.*, vol. 20, no. 6, pp. 2017–2025, Dec. 2013.
[25] Y. Ding, Y. Wang, H. Sun, and Y. Yin, "High-temperature partial discharge characteristics of power module packaging insulation under square pulse with high dv/dt based on down-mixing method," *IEEE Trans. Ind. Electron.*, vol. 70, no. 7, pp. 7334–7342, Jul. 2023.
[26] C. Zheng, Q. Wang, Z. Shen, C. L. Bak, F. F. da Silva, and H. Wang, "Influence of pressure on the PD and induced aging behavior of polyimide insulation under repetitive pulse voltage," *IEEE Trans. Dielectr. Electr. Insul.*, vol. 30, no. 3, pp. 1283–1293, Jun. 2023.
[27] L. Benmamas, P. Teste, E. Odic, G. Krebs, and T. Hamiti, "Contribution to the analysis of PWM inverter parameters influence on the partial discharge inception voltage," *IEEE Trans. Dielectr. Electr. Insul.*, vol. 26, no. 1, pp. 146–152, Feb. 2019.
[28] Z. Guo, A. Q. Huang, R. E. Hebner, G. C. Montanari, and X. Feng, "Characterization of partial discharges in high-frequency transformer under PWM pulses," *IEEE Trans. Power Electron.*, vol. 37, no. 9, pp. 11199–11208, Sep. 2022.
[29] Z. Guo and A. Q. Huang, "Characterizations of partial discharge in modern power electronics," *IEEE J. Emerg. Sel. Topics Power Electron.*, vol. 12, no. 6, pp. 5705–5714, Dec. 2024.
[30] I. M. Jarrar, E. A. Cherney, and S. H. Jayaram, "Effect of repetitive impulse waveform characteristics on partial discharges in type II turn-to-turn insulation," *IEEE Trans. Dielectr. Electr. Insul.*, vol. 29, no. 3, pp. 1183–1190, Jun. 2022.
[31] C. Xia et al., "Multispectral optical partial discharge detection, recognition, and assessment," *IEEE Trans. Instrum. Meas.*, vol. 71, 2022, Art. no. 7002911.
[32] R. Agarwal, H. Li, Z. Guo, and P. Cheetham, "The effects of PWM with high dv/dt on partial discharge and lifetime of medium-frequency transformer for medium-voltage (MV) solid state transformer applications," *IEEE Trans. Ind. Electron.*, vol. 70, no. 4, pp. 3857–3866, Apr. 2023.
[33] Y. Zang et al., "Optical detection method for partial discharge of printed circuit boards in electrified aircraft under various pressures and voltages," *IEEE Trans. Transport. Electrific.*, vol. 8, no. 4, pp. 4668–4677, Dec. 2022.
[34] H. You, Z. Wei, B. Hu, Z. Zhao, R. Na, and J. Wang, "Partial discharge behaviors in power modules under square pulses with ultrafast dv/dt," *IEEE Trans. Power Electron.*, vol. 36, no. 3, pp. 2611–2620, Mar. 2021.
[35] H. D. Ilkhechi and M. H. Samimi, "Applications of the acoustic method in partial discharge measurement: A review," *IEEE Trans. Dielectr. Electr. Insul.*, vol. 28, no. 1, pp. 42–51, Feb. 2021.
[36] H. Xiong et al., "The Ohio State university partial discharge detection platform for electric machine windings driven by PWM voltage excitation," in *Proc. IEEE Elect. Insul. Conf.*, 2019, pp. 517–520.
[37] X. Wei et al., "A robust online junction temperature calibration method for power semiconductors in traction inverter application," *IEEE Trans. Transport. Electrific.*, vol. 11, no. 2, pp. 6602–6614, Apr. 2025.
[38] P. Mathew, M. G. Niasar, and P. Vaessen, "Design of high-frequency fast-rise pulse modulators for lifetime testing of dielectrics," *IEEE Trans. Dielectr. Electr. Insul.*, vol. 30, no. 6, pp. 2798–2808, Dec. 2023.
[39] P. Mathew, "Pulsed ageing of oil-paper: Test modulators and ageing trends," M.S. thesis, Delft University of Technology, Delft, The Netherlands, 2021. [Online]. Available: https://resolver.tudelft.nl/uuid:6551068d-3de4-4fb1-9227-31259052e88a
[40] *Electrical Insulating Materials and Systems—Electrical Measurement of Partial Discharges (PD) Under Short Rise Time and Repetitive Voltage Impulses*, International Electrotechnical Commission, IEC TS 61934, 2011.
[41] R. Arora and W. Mosch, *High Voltage and Electrical Insulation Engineering*. Hoboken, NJ, USA: Wiley, 2022.
[42] Y. Wang et al., "Space-charge accumulation and its impact on high-voltage power module partial discharge under DC and PWM waves: Testing and modeling," *IEEE Trans. Power Electron.*, vol. 36, no. 10, pp. 11097–11108, Oct. 2021.
[43] T. Baumann, B. Fruth, F. Stucki, and H. Zeller, "Field-enhancing defects in polymeric insulators causing dielectric aging," *IEEE Trans. Elect. Insul.*, vol. 24, no. 6, pp. 1071–1076, Dec. 1989.
[44] L. Niemeyer, "A generalized approach to partial discharge modeling," *IEEE Trans. Dielectr. Elect. Insul.*, vol. 2, no. 4, pp. 510–528, Aug. 1995.
[45] H. Okubo, N. Hayakawa, and G. C. Montanari, "Technical development on partial discharge measurement and electrical insulation techniques for low voltage motors driven by voltage inverters," *IEEE Trans. Dielectr. Electr. Insul.*, vol. 14, no. 6, pp. 1516–1530, Dec. 2007.
[46] P. Wang, A. Cavallini, and G. C. Montanari, "Characteristics of PD under square wave voltages and their influence on motor insulation endurance," *IEEE Trans. Dielectr. Electr. Insul.*, vol. 22, no. 6, pp. 3079–3086, Dec. 2015.
[47] M. Ren, M. Dong, C. Zhang, and J. Liu, "Partial discharges in void defect of gas insulated switchgear insulator under standard aperiodic and oscillating switching impulses," *IEEE Trans. Dielectr. Electr. Insul.*, vol. 23, no. 5, pp. 2933–2941, Oct. 2016.
[48] L. Testa, S. Serra, and G. Montanari, "Advanced modeling of electron avalanche process in polymeric dielectric voids: Simulations and experimental validation," *J. Appl. Phys.*, vol. 108, no. 3, 2010, Art. no. 034110.
[49] G. C. Montanari and P. Seri, "About the definition of PDIV and RPDIV in designing insulation systems for rotating machines controlled by inverters," in *Proc. IEEE Elect. Insul. Conf.*, 2018, pp. 554–557.
[50] A. Cavallini and G. Montanari, "Effect of supply voltage frequency on testing of insulation system," *IEEE Trans. Dielectr. Electr. Insul.*, vol. 13, no. 1, pp. 111–121, Feb. 2006.
[51] F. Gutfleisch and L. Niemeyer, "Measurement and simulation of PD in epoxy voids," *IEEE Trans. Dielectr. Electr. Insul.*, vol. 2, no. 5, pp. 729–743, Oct. 1995.
[52] S. Simula, T. Varpula, S. Ikäläinen, H. Seppä, A. Paukku, and K. Niskanen, "Measurement of the dielectric properties of paper," in *Proc. NIP Digit. Fabr. Conf.*, 1998, pp. 157–160.
[53] T. J. A. Hammarström, "Partial discharge characteristics at ultra-short voltage risetimes," *IEEE Trans. Dielectr. Electr. Insul.*, vol. 25, no. 6, pp. 2241–2249, Dec. 2018.
[54] P. Wang, H. Xu, J. Wang, W. Zhou, and A. Cavallini, "The influence of repetitive square wave voltage rise time on partial discharge inception voltage," in *Proc. IEEE Conf. Elect. Insul. Dielectric Phenomena*, 2016, pp. 759–762.
[55] T. J. Hammarstroem, "Influence of voltage overshoot in enamel wire winding insulation systems," in *Proc. IEEE Conf. Elect. Insul. Dielectric Phenomena*, 2023, pp. 1–5.
[56] T. Hammarström, "Overshoot level studies of PD exposure in high voltage motor isolation," *IEEE Trans. Dielectr. Electr. Insul.*, vol. 32, no. 2, pp. 1172–1180, Apr. 2025.

Zhaoxin Wang (Member, IEEE) was born in Henan, China, in 1994. She received the M.S. degree from North China Electric Power University, Hebei, China, in 2020 and the Ph.D. degree from Aalborg University, Aalborg, Denmark, in 2024, all in electrical engineering.

She is currently a Postdoctoral Researcher with Aalborg University, Aalborg, Denmark. She was a Visiting Scholar with the Delft University of Technology (TU Delft), Delft, The Netherlands. Her research interests include multiphysics modeling of high-frequency transformers, life modeling and partial discharge of insulation in power electronics, and EMI filter lifetime and reliability.

Xing Wei (Member, IEEE) received the B.E. degree in electrical engineering and automation from Nanjing Normal University, Nanjing, China, in 2016, the M.E. degree in electrical engineering from Southeast University, Nanjing, China, in 2019, and the Ph.D. degree in power electronics from Aalborg University, Aalborg, Denmark, in 2024.

From 2017 to 2018, he was a Visiting Student with RWTH Aachen University, Aachen, Germany. He is currently a Postdoctoral Researcher with the Department of Energy, Aalborg University. His research interests include the power electronic reliability and the condition and health monitoring for traction inverter applications.

Claus Leth Bak (Senior Member, IEEE) was born in Århus, Denmark, in 1965. He received the B.Sc. (Hons.) degree in electrical power engineering in 1992 and the M.Sc. degree in electrical power engineering from the Department of Energy Technology, Aalborg University, Aalborg, Denmark, in 1994, and the Ph.D. degree from Aalborg University, in 2015. His Ph.D. dissertation was titled "EHV/HV underground cables in the transmission system."

After his studies, he was a Professional Engineer with Electric Power Transmission and Substations with specializations within the area of Power System Protection with the NV Net Transmission System Operator. In 1999, he was an Assistant Professor with the Department of Energy Technology, Aalborg University. He was a Full Professor in 2011. He has supervised/cosupervised +45 Ph.D.'s and +50 M.Sc. theses. He is the author/coauthor of app. 440 publications. His main research areas include corona phenomena on overhead lines, composite transmission towers, power system modeling and transient simulations, underground cable transmission, power system harmonics, power system protection, composite materials for EHV power pylons and HVdc-VSC Offshore Transmission Networks.

Dr. Bak is a Chair of the Danish Cigré National Committee, former member of CIGRE Technical Council and member of Cigré SC C4 AG1 and D1. He was the recipient of the DPSP 2014 best paper award and the PEDG 2016 best paper award. He was also the recipient of the CIGRE Distinguished member award (2020) and CIGRE TC award (2020). He is currently a Head of the Energy Technology Ph.D. program (+ 130 Ph.D.'s) and a Head of the Section of Electric Power Systems and Microgrids and is a member of the Ph.D. board with the Faculty of Engineering and Science.

Filipe Faria da Silva (Senior Member, IEEE) received the M.Sc. degree in electrical and computers engineering from the Instituto Superior Técnico, Lisbon, Portugal, in 2008 and the Ph.D. degree in electric power systems from Aalborg University, Aalborg, Denmark, in 2011.

In 2008, he was with EDP-Labelec, Sacavém, Portugal, and from 2008 to 2011, with Danish TSO Energinet. He is currently an Associate Professor with the Department of Energy Technology, Aalborg University, where he is also Semester Coordinator for the Electrical Power System and High Voltage Engineering Master Program and the Leader of the Modern Power Transmission Systems Research Program. His research interests include power cables, electromagnetic transients and insulation coordination, power quality, network stability, HVdc transmission, and HV phenomena..

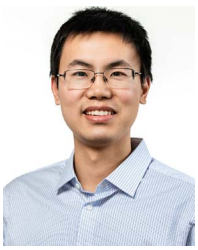

Tianming Luo (Member, IEEE) was born in Jinan, China, in 1993. He received B.E. degree in electrical engineering and automation from Chongqing University, Chongqing, China, in 2015, the M.Sc. degree in high voltage and insulation engineering from China Electric Power Research Institute, Beijing, China, in 2018, and the Ph.D. degree in electrical engineering from the Delft University of Technology, Delft, The Netherlands, in 2025.

He is currently a Postdoctoral Researcher with the Technique University of Denmark, Kongens Lyngby, Denmark. His research interests are multiphysic models of medium-frequency transformers, multiobjective optimization, and insulation performance under medium frequencies.

Weichuan Zhao was born in Changchun, Jilin, China, in 1995. He received the M.Sc. and Ph.D. degrees in electrical power engineering from the Delft University of Technology, Delft, The Netherlands, in 2020 and 2025 respectively.

He is currently a High-Voltage Engineer in Optics11, application team. His research interests include partial discharge monitoring and diagnostics, high-frequency aging of the insulation materials, and high-voltage power electronics.

Peter Vaessen (Member, IEEE) was born in Maasbree, The Netherlands, in 1960. He received the M.Sc. (*cum laude*) degree in electrical power engineering from Eindhoven Technical University, Eindhoven, The Netherlands, in 1985.

He joined KEMA (now a CESI brand), in 1985. In his 35-year career, he held research positions in the field of large power transformers and high-voltage measurement and testing. He has 25 years of experience in (U)HVdc technology and T&D grids with high shares of renewables. He is a Manager innovations with KEMA Laboratories and chairman of the European Distributed Energy Resources Laboratories association (DERlab), as well as member of several national and international working groups. Since 2017, he has been a part-time Professor Hybrid Transmission Systems with TU Delft, Delft, The Netherlands, where he teaches high-voltage technology and HVdc.

Henrik Sørensen received the M.Sc. degree in thermo-mechanical engineering from Aalborg University, Aalborg, Denmark, in 1999, the Ph.D. degree in fluid dynamics/multi phase flows in 2006, and the master's degree in public governance from Aalborg University, in 2021.

He is currently an Associate Professor and the Head of the Section for Thermal Engineering, Department of Energy, Aalborg University. In 2015, he completed the Leadership Development Program with the European Consortium of Innovative Universities, Brussels, Belgium. He has been the Head of Section since 2008. His research interests are fluid mechanics, multiphase flow, and heat transfer.

Mohamad Ghaffarian Niasar (Member, IEEE) was born in Tehran, Iran, in 1984. He received the M.Sc. degree in electrical power engineering from the Sharif University of Technology, Tehran, Iran, in 2008 and the Ph.D. degree in electrical engineering from the Royal Institute of Technology (KTH), Stockholm, Sweden, in 2015.

He is currently an Assistant Professor with High Voltage Technologies Group, Delft University of Technology, Delft, The Netherlands. His main research interests are aging of insulation material, HVdc insulation system, high-frequency power transformers, and multiphysics modeling of power components.